European Journal of Medical Research

RESEARCH

Open Access

Identification of RBM15 as a prognostic biomarker in prostate cancer involving the regulation of prognostic m6A-related lncRNAs

Bintao Hu[1,2†], Dongxu Lin[1†], Zhicheng Liu[3†], Ruibao Chen[1], Jihong Liu[1], Yue Wu[1*] and Tao Wang[1,2*]

Abstract

Background Long noncoding RNAs (lncRNAs) and N6-methyladenosine (m6A) modification of RNA play pivotal roles in tumorigenesis and cancer progression. However, knowledge regarding the expression patterns of m6A-related lncRNAs and their corresponding m6A regulators in prostate cancer (PCa) is limited. This study aimed to delineate the landscape of m6A-related lncRNAs, develop a predictive model, and identify the critical m6A regulators of prognostic lncRNAs in PCa.

Methods Clinical and transcriptome data of PCa patients were downloaded from The Cancer Genome Atlas (TCGA) database. Prognostic m6A-related lncRNAs were subsequently identified through Pearson correlation and univariate Cox regression analyses. The prognostic lncRNAs were clustered into two groups by consensus clustering analysis, and a risk signature model was constructed using least absolute shrinkage and selection operator (LASSO) regression analysis of the lncRNAs. This model was evaluated using survival, clinicopathological, and immunological analyses. Furthermore, based on the constructed lncRNA-m6A regulatory network and RT-qPCR results, RBM15 was identified as a critical regulator of m6A-related lncRNAs. The biological roles of RBM15 in PCa were explored through bioinformatics analysis and biological experiments.

Results Thirty-four prognostic m6A-related lncRNAs were identified and categorized into two clusters with different expression patterns and survival outcomes in PCa patients. Seven m6A lncRNAs (AC105345.1, AL354989.1, AC138028.4, AC022211.1, AC020558.2, AC004076.2, and LINC02666) were selected to construct a risk signature with robust predictive ability for overall survival and were correlated with clinicopathological characteristics and the immune microenvironment of PCa patients. Among them, LINC02666 and AC022211.1 were regulated by RBM15. In addition, RBM15 expression correlated with PCa progression, survival, and the immune response. Patients with elevated RBM15 expression were more susceptible to the drug AMG-232. Moreover, silencing RBM15 decreased the viability of PCa cells and promoted apoptosis.

†Bintao Hu, Dongxu Lin and Zhicheng Liu contributed equally to this work.

*Correspondence:
Yue Wu
wuyuetjm@163.com
Tao Wang
tjhwt@126.com
Full list of author information is available at the end of the article

Conclusion RBM15 is involved in the regulation of prognostic lncRNAs in the risk signature and has a robust predictive ability for PCa, making it a promising biomarker in PCa.

Keywords Biomarker, LASSO regression, Long noncoding RNAs, M6A methylation, Prostate cancer, RBM15

Introduction

Prostate cancer (PCa), with an incidence surpassing 1,400,000 newly diagnosed cases and 375,000 deaths worldwide in 2020, is the second most prevalent malignancy and the fifth most common cause of cancer death among the male population [1]. Although prostate-specific antigen (PSA) is a convenient biomarker for managing PCa, it has a predictive accuracy of only 25–40% [2]. Hence, exploring novel and reliable biomarkers for assessing patient prognosis and therapeutic efficacy is imperative in facilitating the implementation of tailored therapy.

Long noncoding RNAs (lncRNAs), which constitute the major component of noncoding RNAs, are generally defined as RNA transcripts exceeding 200 nucleotides. Extensive research indicates that lncRNAs are significantly involved in various biological processes, including transcriptional and post-transcriptional regulation [3], oncogenesis and metastasis [4], and the immune response [5]. Certain lncRNAs can form regulatory networks associated with diseases, thereby contributing to the pathogenesis of these diseases [6]. Moreover, numerous lncRNAs, such as MAFG-AS1, CAT179, CAT1796, CAT2064, and CAT2042, have been recognized as potential markers for diagnosing and predicting the prognosis of PCa patients [7–9]. Notably, the intracellular functions of lncRNAs are regulated by N6-methyladenosine (m6A)-related proteins, and the potential synergistic interactions between these proteins strongly influence cancer progression [10].

M6A, which refers to the addition of a methyl group to the adenine base at position N6, is a predominant epigenetic modification of RNAs [11]. Various methylation enzymes, such as methyltransferases (writers), binding proteins (readers), and demethylases (erasers), elaborately regulate the dynamic and reversible process of m6A modification [12]. M6A regulator-mediated RNA modifications can influence physiological and pathological processes across various systems. For instance, it has been reported that m6A modifications are involved not only in hematopoietic and brain development [13] but also in the regulation of the immune microenvironment in periodontal disease [14]. While most studies have concentrated on the m6A modification of mRNAs, recent evidence suggests that m6A methylation also impacts the synthesis and function of lncRNAs. Thus, an integrated landscape of lncRNAs associated with m6A will enhance our understanding of m6A-based strategies for cancer treatment.

In this study, we established a risk signature for PCa patients based on prognostic m6A-related lncRNAs, and conducted a comprehensive analysis of survival outcomes, clinical characteristics, and the immune microenvironment. Experimentation and correlation analysis revealed that the m6A regulator RBM15 interacted with the identified prognostic lncRNAs and affected survival outcomes, clinical progression, and the immune microenvironment of PCa patients. Overall, our findings suggest that RBM15 is a promising biomarker and potential therapeutic target that significantly influences tumor progression and immune responsiveness in PCa patients.

Methods

Data acquisition and processing

TCGA database was utilized to download the transcriptome data expressed as fragments per kilobase of transcript per million mapped reads (FPKM) and clinical data of PCa patients. A total of 553 clinical samples were obtained, consisting of 501 PCa samples and 52 normal samples. Duplicate genes in the transcriptome and genes with zero expression in each sample were removed to obtain the gene expression profiles of the TCGA-PRAD cohort. LncRNA expression profiles were subsequently extracted according to the gene annotations of the lncRNAs from the GENCODE database. Twenty-seven m6A regulators were identified by searching related literatures from the PubMed database. Similarly, the corresponding expression profiles were acquired based on the 27 m6A regulators. Pearson correlation analysis between 27 m6A regulators and lncRNAs was performed with the screening criteria of $p < 0.001$ and $|R| > 0.4$ to identify m6A-related lncRNAs. Prognostic m6A-related lncRNAs were identified by univariate Cox regression analysis ($p < 0.001$) with the R package "survival".

Consensus clustering analysis for the prognostic m6A-related lncRNAs

Based on the consensus level of the prognostic m6A-related lncRNAs, samples from the TCGA-PRAD cohort were clustered into different m6A patterns using the R package "ConsensusClusterPlus". The appropriate number of clusters was selected based on a low coefficient of variation, no discernible growth in the cumulative distribution function (CDF) curve, and good consistency

of the clusters. The fitness of the classifications was assessed using principal component analysis (PCA), which was conducted with the R packages "FactoMineR" and "factoextra". Kaplan–Meier (K–M) survival analysis was performed using the "survminer" package to assess variations in overall survival outcomes among different clusters. The correlations between different clusters and clinical characteristics, such as Gleason score, pathological T/N stage, and age, were analyzed using the Chi-square test.

Development of a risk signature using prognostic m6A-related lncRNAs

Using the glmnet R package, LASSO regression analysis was conducted to identify the most informative genes among the prognostic m6A-related lncRNAs. The most informative genes were utilized to construct a risk signature. The risk signature was calculated using the following formula: risk score = $\sum$ (lncRNA expression × corresponding coefficient). After calculating each sample's risk score, the samples were split into low-risk and high-risk groups according to the median risk score. To validate the predictive capacity of the risk signature, receiver operating characteristic (ROC) and K–M survival analyses were performed using the R packages "survival" and "timeROC". In addition, the risk scores of patients in subgroups with different clinicopathological characteristics were compared using the "stat_compare_means" function of the "ggpubr" package. Univariate and multivariate Cox regression analyses were performed using the R package "survival" on risk scores and several clinicopathological characteristics, including the Gleason score, pathological T/N stage, and age, to identify the independent prognostic factors of PCa.

Analysis of the tumor microenvironment, tumor mutation burden (TMB), and immune checkpoints in PCa samples

The infiltration abundances of 22 immune cells were determined using the CIBERSORT method for each PCa sample [15]. A comparison of infiltration abundance was made using the "stat_compare_means" function of the "ggpubr" package between different clusters or between the high- and low-expression RBM15 groups. Pearson correlation analysis was utilized to analyze the relationship between RBM15 expression or the risk score and the infiltration level of immune cells. The immunological microenvironment of PCa tissues was also investigated using the ESTIMATE algorithm [16]. The calculated stromal score, immune score, and ESTIMATE score were used to evaluate the overall immunological state of the PCa samples. In addition, the correlation between RBM15 and checkpoint genes was assessed with Pearson correlation analysis. Immunophenoscores (IPSs) can be used to quantitatively evaluate the efficacy of checkpoint inhibitors. The Cancer Immunome Atlas (TCIA) database was used to obtain IPS data for TCGA-PRAD patients. The immune checkpoints PD-1 and CTLA-4 were used to predict immunotherapy efficacy. Furthermore, as a biomarker for predicting immunotherapy efficacy, the association between the TMB and RBM15 expression was analyzed using Pearson correlation analysis.

Drug sensitivity analysis

The CellMiner database is a powerful tool for exploring the association of gene expression with drug sensitivity [17]. First, the processed dataset of the CellMiner database, which included RNA-seq and DTP NCI-60 (compound activity) data, was downloaded. Next, the drugs that have been clinically tested and approved by the FDA were selected for Pearson correlation analysis with specific genes. The missing drug data were filled in by the R package "impute".

Bioinformatics analysis of RBM15 function

First, we analyzed RBM15 expression in tumor and normal samples. The RNA expression of RBM15 in TCGA-PRAD samples was determined from the downloaded transcriptome data. The differential expression of RBM15 between tumor samples and unpaired or paired normal samples was compared using the stat_compare_means function. In addition, the Human Protein Atlas (HPA) and Cancer Cell Line Encyclopedia (CCLE) databases were utilized to analyze RBM15 expression in normal and tumor samples at the protein and mRNA levels, respectively. The differential expression of RBM15 among subgroups with different clinical characteristics, including Gleason score, pathological T/N stage, and age, was compared using the stat_compare_means function. Based on the median expression of RBM15, PCa samples were split into high- and low-expression groups. Utilizing the R package "Limma", differential expression analysis was conducted for the two groups. The obtained DEGs were used to construct a heatmap with the R package "pheatmap". In addition, using the R package "clusterprofiler", Kyoto Encyclopedia of Genes and Genomes (KEGG) and Gene Ontology (GO) enrichment analyses were performed. To further validate the role of RBM15 in PCa, external datasets, including GSE46602, GSE54460, GSE94767, GSE74367, GSE150807, GSE151083, and the DKFZ cohort, were obtained and analyzed from the GEO and cBioPortal databases.

Cell culture

Human prostate nontumoral epithelial cells (BPH-1 and RWPE-1) and tumoral cell lines (DU145, PC-3, 22Rv1,

C4-2, C4-2B, and LNCaP) were purchased from Procell Life Science & Technology Co., Ltd (Wuhan, China) or the American Type Culture Collection (Manassas, VA, USA). RWPE-1 cells were maintained in prostate epithelial cell medium supplemented with 1% PEpiCGS (ScienCell, Carlsbad, USA). PC-3 cells were maintained in F12K medium that contained 10% fetal bovine serum (FBS). The other cells were cultured in RPMI-1640 medium supplemented with 10% FBS. All the cells were incubated in a controlled environment at 37 °C and a CO_2 concentration of 5%. The enzalutamide-resistant cell line C4-2B EnzR was generated by selecting the C4-2B clones that survived in 20 μM enzalutamide.

Cell transfection

Small interfering RNA (siRNA) targeting RBM15 (called siRBM15) and random scrambled siRNA (called siNC), which were synthesized by Genomeditech (Shanghai, China), were used to reduce RBM15 expression. The siRNA sequences used are listed in Supplementary Table 1. Figure S7 demonstrates that the cell transfection achieved high efficiency. LINC02666 and AC022211.1 sequences were inserted into the pcDNA 3.1 (+) vector to construct overexpression plasmids, which were synthesized by General Biol Co., Ltd. Cells were cultured in six-well plates until the confluency reached 60–80%, and 100 nM of siRNA or 2.5 μg plasmid was transfected into the cells using Lipofectamine 3000 (Invitrogen, Carlsbad, USA).

RT-qPCR

A SteadyPure RNA Extraction Kit (Accurate Biology, Changsha, China) was utilized to extract RNA from the samples. Afterward, cDNA was synthesized from the extracted RNA using a cDNA Synthesis Kit (Yeasen, Shanghai, China) and SYBR Green Master Mix reagents purchased from Yeasen Biotechnology (Shanghai) Co., Ltd. were used for detection. The primers sequences used are listed in Supplementary Table 2.

Western blot

Cell samples were lysed using RIPA buffer (BOSTER Biological Technology Co., Ltd., Wuhan, China) and ultrasonicated to obtain protein samples. Then 20 μg of total protein was subjected to electrophoresis and electrotransfer process, and proteins were transferred onto PVDF membranes. Subsequently, the membranes were blocked with nonfat milk and incubated with anti-β-actin (ABclonal, Wuhan, China), anti-RBM15 (Proteintech, Wuhan, China), or anti-GAPDH (Boster, Wuhan, China) antibodies at 4 °C overnight. Afterward, the membranes were incubated with HRP-conjugated AffiniPure goat anti-rabbit IgG (H + L) (Boster, Wuhan, China) at room temperature for 1 h. Finally, the proteins were detected using an enhanced chemiluminescence (ECL) kit (Servicebio, Wuhan, China).

Immunohistochemistry (IHC)

PCa and adjacent normal prostate tissues from patients who underwent radical prostatectomy were acquired. The Ethics Committee of Tongji Hospital (TJ-IRB20221316) granted approval for this investigation. The samples were fixed, paraffinized and sliced into sections. After being deparaffinized and rehydrated, the paraffinized sections were treated with 3% H_2O_2 and blocked with goat serum. Finally, the sections were sequentially incubated with a specific primary antibody, secondary antibody, and DAB solution.

Cell viability detection

Approximately 5,000 cells/well were seeded in 96-well plates. The following day, the cells were subjected to treatment with RBM15-targeting siRNA. After 96 h of treatment, the cells were incubated for 2 h with Cell Counting Kit-8 solution from Yeasen Biotechnology Co., Ltd. The cell viability was measured by reading the absorbance at 450 nm.

Flow cytometry for cell apoptosis

PCa cells were cultured in six-well plates and transfected with siRNA targeting RBM15 when the cell confluence reached approximately 60 ~ 70%. After transfection for 72 h, the cells were collected and stained with PI and Annexin V-FITC solution (Yeasen, Shanghai, China) for flow cytometry to determine the cell apoptosis rate.

Statistical analysis

R 4.2.1 or GraphPad Prism 9.5.0 software was utilized to conduct the statistical analyses. The statistical results were considered statistically significant when p was less than 0.05. The Pearson correlation analysis was performed to analyze the associations between two groups. Group differences were assessed using various statistical tests, including one-way analysis of variance, Wilcoxon signed-rank test, Mann–Whitney U test, or independent t test.

Results

Identification and evaluation of prognostic m6A-related lncRNAs in PCa

Figure 1 presents the entire flowchart of this study. First, the clinical and transcriptome data of PCa patients were acquired from TCGA database. Afterward, the lncRNA expression profiles were obtained using GENCODE annotations. To obtain comprehensive information on m6A regulators, we searched relevant literature from the

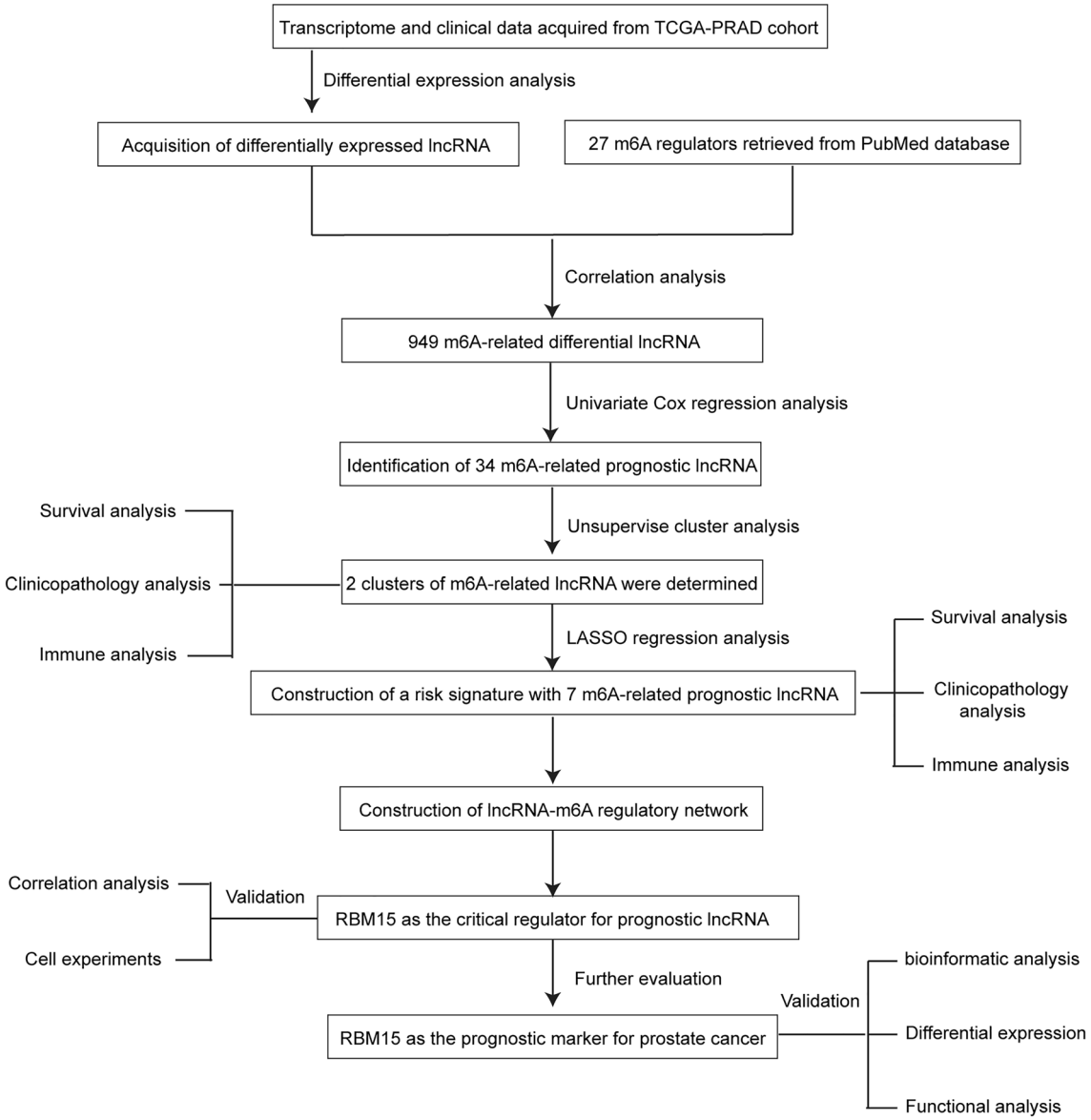

Fig. 1 The flowchart depicts the research strategy of this study

PubMed database. As a result, 11 writers, 14 readers, and 2 erasers were identified (Supplementary Table 3). Subsequently, correlation analysis was performed between the lncRNAs and 27 m6A regulators to identify m6A-related lncRNAs. The network of lncRNAs and m6A regulators is shown in Fig. 2A. A total of 949 significant m6A-related lncRNAs were identified ($p < 0.001$ and $|R| > 0.4$). Furthermore, univariate Cox regression analysis of these lncRNAs was conducted to obtain prognostic m6A-related lncRNAs. As a result, 34 prognostic m6A lncRNAs were identified ($p < 0.001$). The corresponding hazard ratios are displayed in Fig. 2B. Figure 2C shows the differential expression of the prognostic lncRNAs between normal and tumor samples. All 34 prognostic lncRNAs exhibited significant differences.

To investigate the associations of the phenotypes of m6A-related lncRNAs with clinical features, a consensus clustering analysis was performed. After the analysis of the consensus clustering CDF and relative change in the area under the CDF curves with k ranging from 2 to 9 (Fig. S1A) and the consensus clustering matrix, $k = 2$ was determined to be the optimal number of clusters (Fig. 2D). Two cluster patterns were confirmed to be clearly distinguished by PCA (Fig. S1B). Strikingly, the

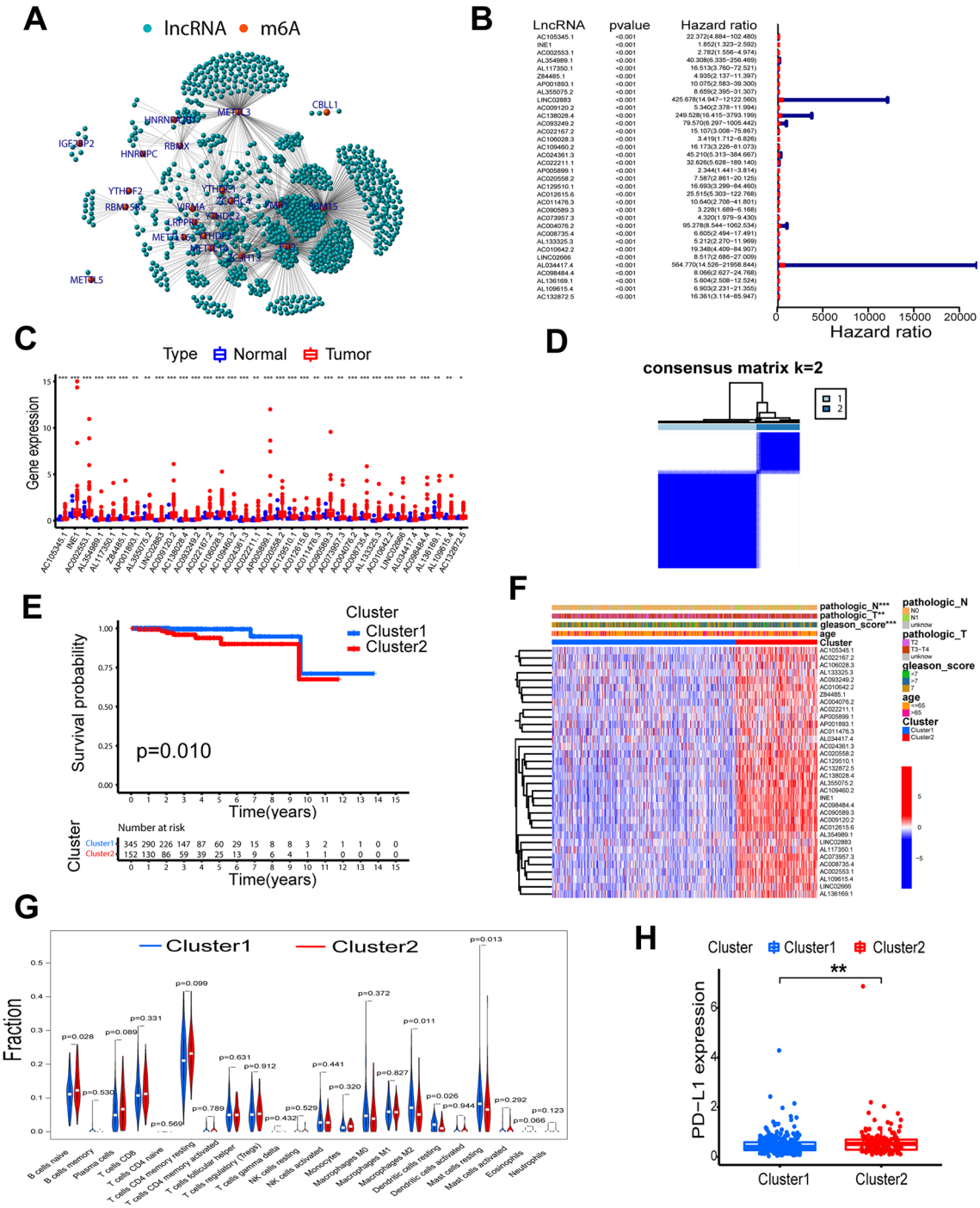

Fig. 2 Identification and evaluation of prognostic m6A-related lncRNAs in PCa. **A** The correlation atlas between m6A regulators and m6A-related lncRNAs. **B** Thirty-four prognostic m6A-related lncRNAs were identified by univariate Cox regression analysis. **C** The differential expression of 34 prognostic m6A lncRNAs in normal and tumor samples. **D** Consensus clustering analysis of the prognostic lncRNAs. **E** Survival analysis of patients in the two clusters. **F** Heatmap showing the correlations between clusters and pathological T and N stage and Gleason score. **G** Violin plot demonstrating the difference in infiltrating immune cells among the different clusters. **H** The differential expression of PD-L1 in different clusters

survival probability of patients in Cluster 2 was inferior to that of patients in Cluster 1 (Fig. 2E). The two cluster patterns exhibited significant correlations with the pathological T/N stage and Gleason score (Fig. 2F). In addition, differences in the expression of the immune checkpoint PD-L1 and immune cell infiltration were compared among the different cluster patterns. The results demonstrated that among the 22 immune cell subpopulations, 4 were significantly different between the 2 clusters: naïve B cells, resting mast cells, resting dendritic cells, and M2 macrophages (Fig. 2G). Cluster 2 had significantly greater PD-L1 expression, which might have contributed to the lower survival probability (Fig. 2H).

Construction and evaluation of a risk signature utilizing prognostic lncRNAs

LASSO regression analysis was conducted on the 34 prognostic m6A-related lncRNAs to identify the optimal pattern of gene combinations. Seven m6A-related lncRNAs were screened out and utilized for developing a risk signature. The m6A lncRNAs in the risk signature (RS-lncRNAs) were AC105345.1, AL354989.1, AC138028.4, AC022211.1, AC020558.2, AC004076.2, and LINC02666. Figure 3A and Figure S2A present evidence of λ selection. Supplementary Table 4 displays the coefficients of the seven m6A-related lncRNAs. Subsequently, the PCa samples in the TCGA cohort were classified into high- or low-risk groups using the median risk scores. Figure S2B shows the significant differences between the low- and high-risk groups via PCA. Figure 3C reveals that the expression levels of 7 RS-lncRNAs were significantly elevated in the high-risk group. Patients in the high-risk group had greater proportions of deaths and shorter survival times than patients in the low-risk group (Fig. 3B). Consistently, survival analysis indicated that the high-risk group tended to have poorer survival outcomes (Fig. 3D). Furthermore, ROC curve analysis of the prognostic signature revealed its strong ability to predict survival, with AUC values of 1.000, 0.889, and 0.833 for 1 year, 3 years, and 5 years, respectively (Fig. 3E). Furthermore, to assess the prediction capacity of the prognostic signature in PCa samples with various clinical characteristics, the risk scores of patients in subgroups with distinct Gleason scores or pathologic T/N stages were compared. As shown in Fig. 3F, the risk scores of the subgroup with a Gleason score > 7 were significantly greater than those of the subgroup with a Gleason score < 7 or 7, and as the pathological T/N stage progressed, the risk score significantly increased. Moreover, Cluster 2 had a higher risk score. The above findings demonstrated that the risk score had good predictive ability for PCa prognosis. Furthermore, univariate and multivariate Cox regression analyses for the Gleason score, pathological T/N stage, age, and risk score demonstrated that the risk score was an independent risk factor for PCa patients (Fig. 3G). In addition, correlation analysis between the infiltration of immune cells and the risk score was conducted. As shown in Fig. 3H, the risk score was negatively correlated with resting mast cells and positively correlated with memory resting CD4 + T cells, activated mast cells, and naïve B cells.

Identification of RBM15 as the critical regulator of prognostic m6A-related lncRNAs from the risk signature

Seven RS-lncRNAs were shown to have a robust ability to predict the prognosis of PCa patients based on the aforementioned analysis. Furthermore, to analyze the critical upstream regulators of the RS-lncRNAs, correlation analysis between the RS-lncRNAs and the corresponding m6A regulators was performed. As shown in Fig. 4A, most of the RS-lncRNAs correlated with METTL3 or RBM15. Given the extensive research on METTL3 in PCa and the limited studies concerning RBM15 in this context, our analysis subsequently focused on RBM15. Figure 4B shows that RBM15 and 4 RS-lncRNAs, AC004076.2, AL354989.1, LINC02666, and AC022211.1, had strong associations, with Pearson correlation coefficients all above 0.4. To verify the regulatory role of RBM15 in RS-lncRNAs, siRNAs targeting the RBM15 gene were synthesized. Figure 4C, D shows the knockdown efficiency of the RBM15 gene at the RNA and protein levels, respectively. After confirming a good knockdown effect on RBM15, changes in LINC02666 and AC022211.1 expression in DU145 and 22Rv1 cells were detected. Similarly, the expression of LINC02666 and AC022211.1 was downregulated after RBM15 knockdown (Fig. 4E, F), which revealed that RBM15 was the critical regulator of RS-lncRNAs.

Bioinformatic analysis of the role of RBM15 in PCa

As the risk signature constructed from RS-lncRNAs had robust predictive power for the prognosis of PCa patients and RBM15 was identified as the critical regulator of RS-lncRNAs, RBM15 might contribute to PCa carcinogenesis and development. Therefore, we conducted a bioinformatic analysis of RBM15 in the TCGA cohort. RBM15 was significantly more highly expressed in tumor samples than in unpaired and paired samples (Fig. 5A, B). Based on the median expression of RBM15 in the TCGA cohort, the expression of RBM15 was divided into two levels, namely, high- and low-level subgroups. Survival analysis for progression-free survival indicated that the high-level subgroup had a poor outcome (Fig. 5C). To further verify the role of RBM15 in PCa, the expression of RBM15 in subgroups with different clinical characteristics was compared. Comparisons of age, pathological N

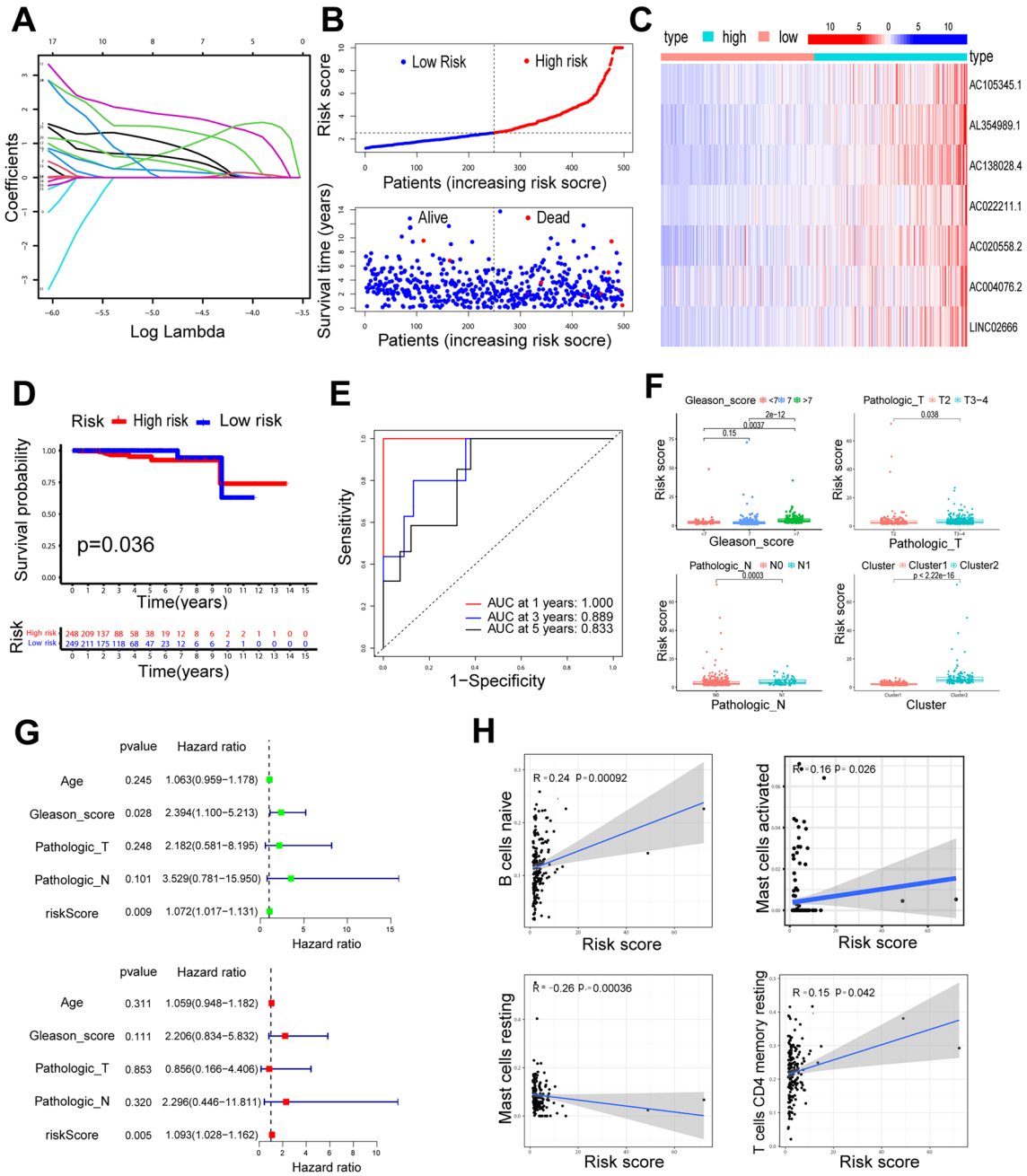

Fig. 3 Construction and evaluation of the risk signature based on prognostic lncRNAs. **A** The coefficients of the prognostic m6A lncRNAs according to LASSO regression analysis. **B** The distribution of survival time and risk scores in PCa patients. **C** Heatmap showing the differences in the expression of RS-lncRNAs between the high- and low-risk groups. **D** The difference in survival probability between the high- and low-risk groups. **E** Time-dependent ROC curve analysis to evaluate the accuracy of the risk signature. **F** Differences in risk scores among the different subgroups. **G** Univariate and multivariate Cox regression analyses for age, Gleason score, pathological T/N stage, and risk score. **H** Correlation analysis between the risk score and infiltrating immune cells

stage, pathological T stage, and Gleason score revealed that RBM15 expression significantly increased with PCa progression (Fig. 5D). To enhance the robustness of the analysis results, we utilized the GSE46602, GSE54460, and GSE94767 datasets obtained from the GEO database, as well as the DKFZ cohort obtained from the cBioPortal website, to investigate the role of RBM15 in PCa. The results indicate that RBM15 is associated with PCa progression (Fig. 5E) and prognosis (Fig. 5F). Furthermore, to explore the role of RBM15 in different types of PCa,

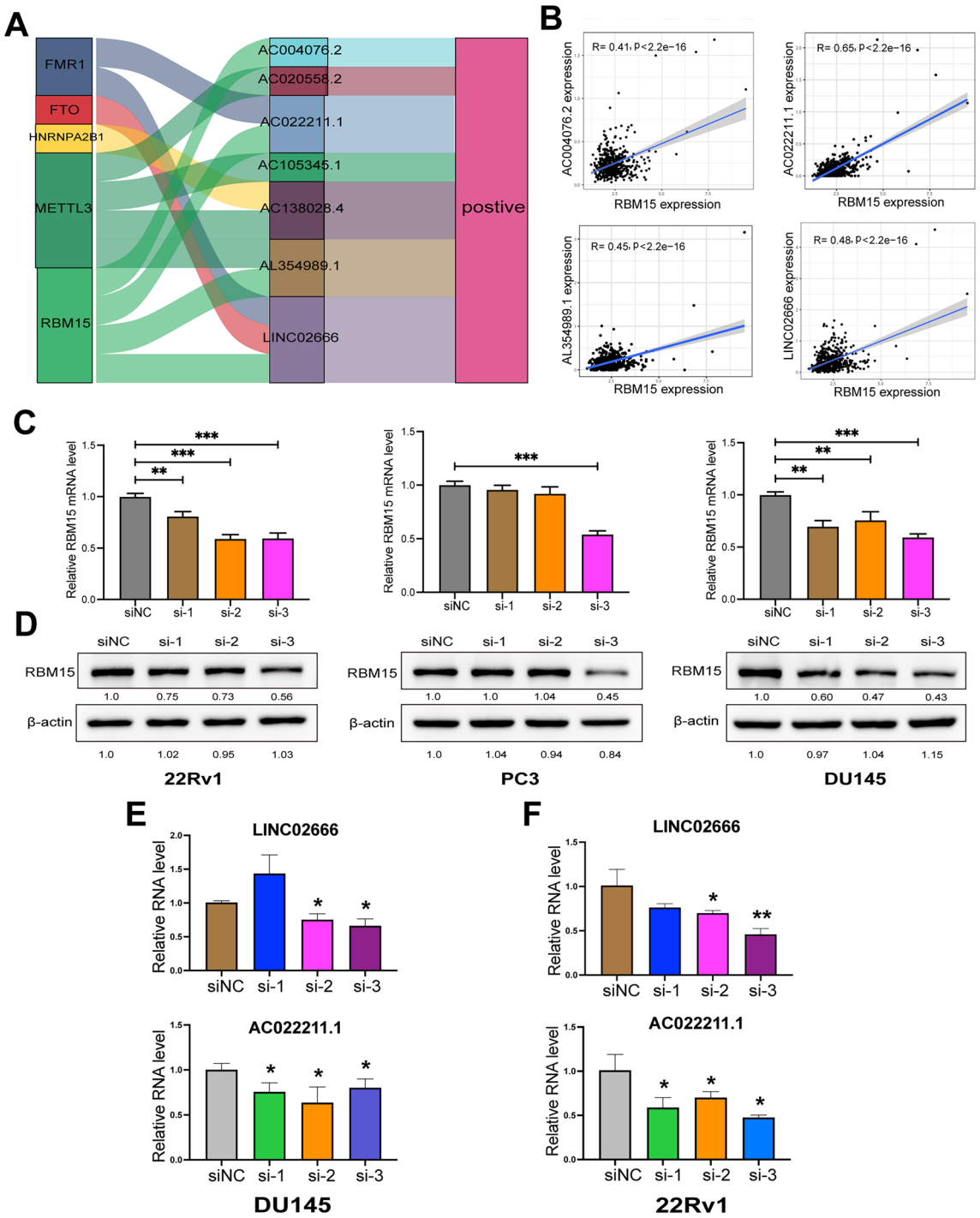

Fig. 4 Identification of RBM15 as the critical regulator of prognostic m6A lncRNAs. **A** Sankey plot displaying the link between m6A regulators and prognostic m6A lncRNAs in the risk signature. **B** Correlation analysis between RBM15 and prognostic m6A-related lncRNAs in the risk signature. **C** Assessment of the knockdown efficiency of the RBM15 gene by siRNA via RT-qPCR. **D** Western blot demonstrating the knockdown efficiency of the RBM15 gene by siRNA. **E**, **F** Changes in the expression of LINC02666 and AC022211.1 in DU145 **E** and 22Rv1 **F** cells following RBM15 gene knockdown. Si-1, si-2, and si-3 represent the three siRNA sequences targeting the RBM15 gene. siNC represents the negative control

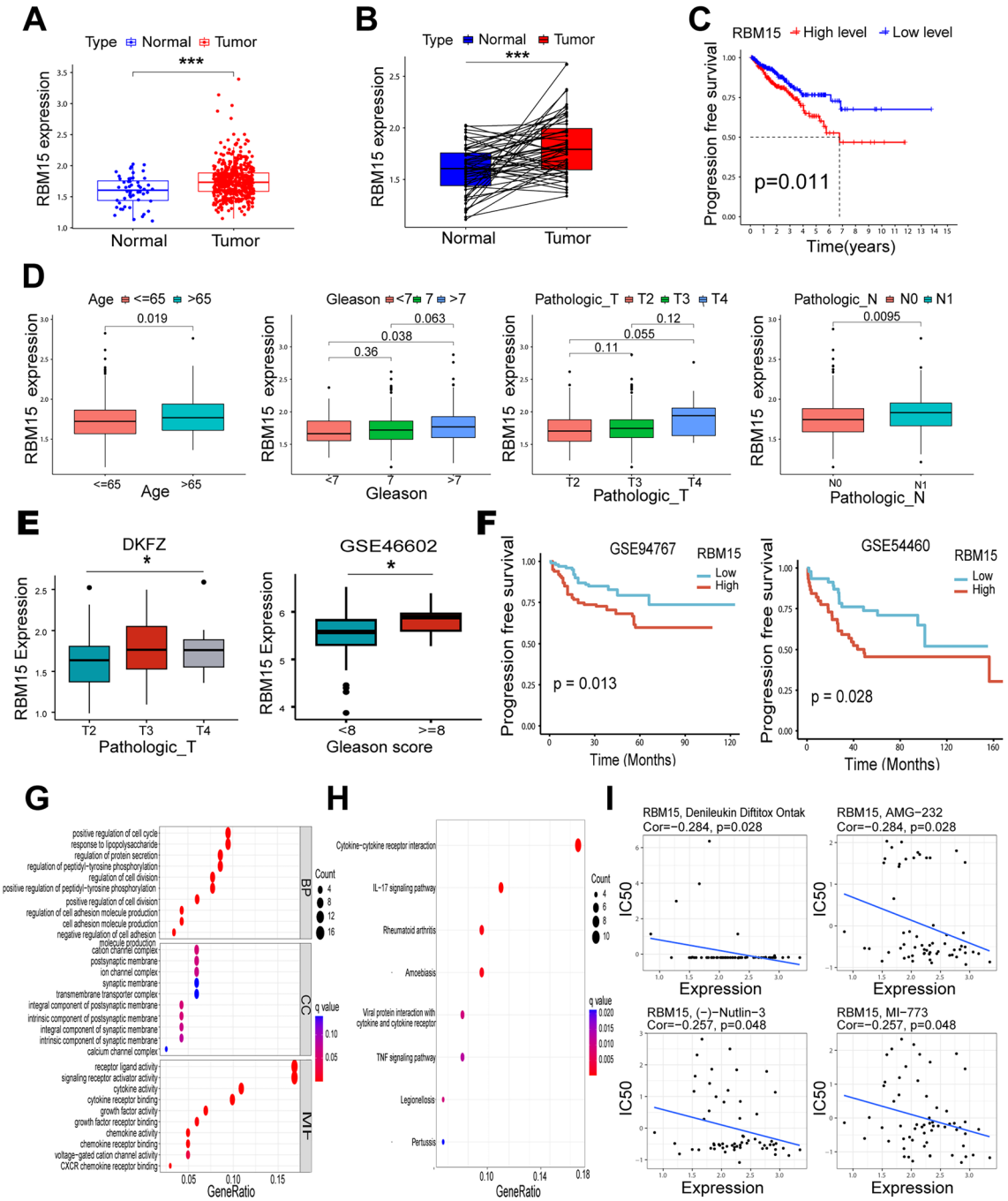

Fig. 5 Bioinformatic analysis of the prognostic role of RBM15 in PCa and the underlying mechanisms. **A** The expression of RBM15 in normal and tumor samples from the TCGA cohort. **B** RBM15 expression in paired samples from the TCGA cohort. **C** Survival analysis according to the RBM15 expression level in TCGA cohort. **D** Differential expression of RBM15 among subgroups with different clinical characteristics, including age, Gleason score, pathological T stage, and pathological N stage in TCGA cohort. **E** Differential expression of RBM15 among subgroups with different pathologic T stages and Gleason scores in the DKFZ and GSE46602 datasets. **F** Survival differences among subgroups with different RBM15 expression levels in the GSE94767 and GSE54460 datasets. **G** GO enrichment analysis of the DEGs in the subgroups with varying RBM15 expression levels. **H** KEGG enrichment analysis of the DEGs in the subgroups with different RBM15 expression levels. **I** Correlation analysis between RBM15 and drugs in the CellMiner

external datasets, including GSE74367, GSE150807, and GSE151083, were obtained and analyzed. Analysis of the GSE74367 dataset showed that RBM15 expression is significantly greater in CRPC tissues than in primary PCa tissues (Fig. S4A). The GSE150807 and GSE151083 datasets indicated that RBM15 expression increases as LNCaP and C4-2B PCa cell lines transition from enzalutamide sensitive to enzalutamide resistant (Fig. S4B). Taken together, these results suggest that RBM15 is involved in the castration resistance of PCa.

Furthermore, to explore the mechanism involving RBM15 in PCa, differentially expressed genes (DEGs) between the high- and low-RBM15 groups were identified with filtering conditions of $|\log FC| > 1$ and $p < 0.05$. The heatmap in Fig. S3A displays the 50 most downregulated and upregulated DEGs. GO enrichment analysis of the DEGs revealed that RBM15 was involved in the regulation of cell division, the cell cycle, and cell adhesion molecule production, which revealed that RBM15 expression might affect the growth and migration of PCa cells (Fig. 5G). KEGG analysis revealed that RBM15 was involved in cytokine–cytokine receptor interactions, the IL-17 signaling pathway, and rheumatoid arthritis (Fig. 5H), which revealed that RBM15 might be related to the immune environment in PCa. In addition, drug sensitivity analysis was performed to discover effective drugs targeting RBM15. The drugs from the CellMiner database were subjected to correlation analysis with RBM15. According to the filter condition of $p < 0.01$, four drugs, Denileukin Diftitox, AMG-232, Nutlin-3, and MI-773, were significantly associated with RBM15 (Fig. 5I). Moreover, cells with high-RBM15 expression tended to be sensitive to AMG-232 (Fig. S3B).

Immune analysis for the association of RBM15 expression with tumor immunity

Under the prompts of the KEGG enrichment analysis, we further conducted immune analysis to investigate the relationship between RBM15 expression and tumor immunity. Immune cells and stromal cells are essential for tumor development and progression in the tumor environment (TME). The high-RBM15 subgroup exhibited significant differences in immune scores (Fig. 6A). Furthermore, the association between RBM15 expression and the level of immune infiltration was determined. Figure 6B shows that RBM15 was positively associated with naïve B cells, resting memory CD4 + T cells, and activated mast cells but was negatively associated with activated NK cells and resting mast cells. In addition, the differences in immune infiltration between the high- and low-RBM15 groups were analyzed. The levels of resting mast cells, activated NK cells, and infiltrating regulatory T cells in the high-RBM15 subgroup were significantly lower than those in the low-RBM15 subgroup (Fig. 6C).

Immunotherapy targeting immune checkpoints is effective in PCa patients. A correlation analysis was conducted between RBM15 and immune checkpoints. The immune checkpoints were strongly correlated with RBM15 based on the screening criterion of $p < 0.001$, and the corresponding Pearson coefficients are displayed in Fig. 6D. RBM15 was significantly correlated with CTLA-4. As the immunophenoscore (IPS) can be used to quantitatively evaluate the efficacy of checkpoint inhibitors, the IPS of patients in the low- and high-RBM15 groups was compared based on the CTLA-4 and PD-1 expression. The comparison indicated that only the IPS of CTLA-4-negative and PD-1-negative patients significantly differed between the low- and high-RBM15 groups (Fig. 6E). Moreover, the tumor mutation burden (TMB) can be used to predict the immune response. Correlation analysis between RBM15 expression and TMB indicated that RBM15 was positively associated with TMB (Fig. 6F).

Experimental validation of the biological role of RBM15 in PCa

The aforementioned analysis revealed that RBM15 is a good predictor of PCa prognosis. To verify the biological role of RBM15, the expression of RBM15 in PCa cells and tissues was first examined based on the results from public databases (CCLE and HPA databases) and experimental examinations (RT-qPCR, western blot, and IHC analysis). Figure 7A indicates that the RNA level of RBM15 in most PCa cells was greater than that in benign prostatic hyperplasia cells (BPH-1). Consistent with these findings, Fig. 7B, C shows that compared to that in normal prostate epithelial cells, RBM15 expression was greater in almost all PCa cells tested. Regarding the PCa tissues, the IHC results from the analysis of the HPA database (Fig. 7D) and the detection of PCa tissues (Fig. 7E) showed that the level of RBM15 expression in the tumors was greater than that in the normal tissue. To further investigate the biological function of RBM15 in PCa, we assessed the impact of RBM15 expression on the viability and apoptosis of PCa cells. As shown in Fig. 7F, the viability of 22Rv1, DU145, and PC-3 cells significantly decreased after RBM15 knockdown. Moreover, the apoptosis rates of 22Rv1 and DU145 cells were significantly increased after RBM15 knockdown (Fig. 7G). Based on the aforementioned findings, the relationships among RBM15, RBM15-regulated m6A lncRNAs (LINC02666 and AC022211.1), and prostate cancer were investigated. We knocked down RBM15 expression while overexpressing the regulated lncRNAs and assessed changes in cell viability using the CCK-8 assay. The results demonstrated

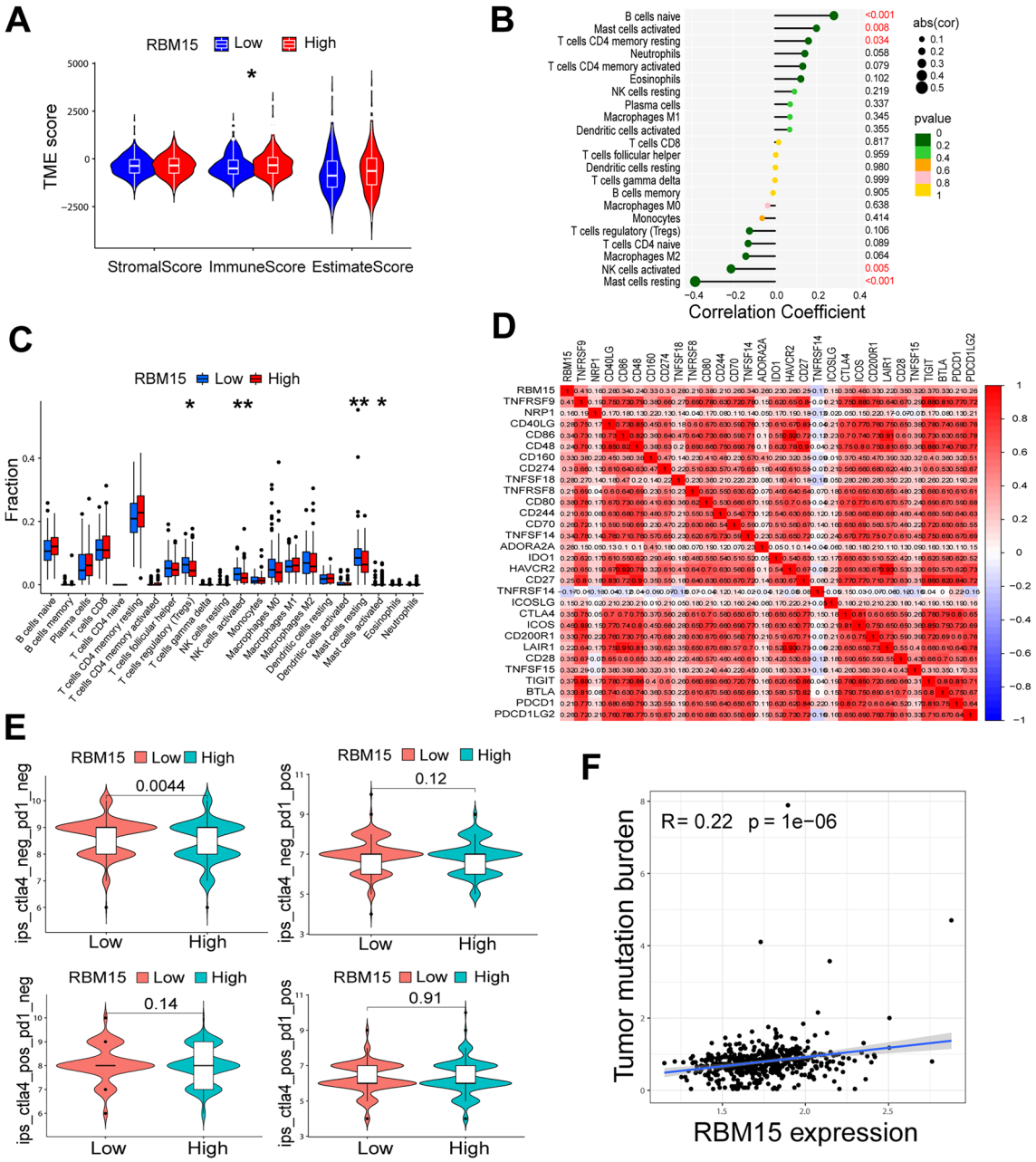

Fig. 6. Immune analysis of RBM15 in PCa. **A** Differences in stromal scores, immune scores, and ESTIMATE scores between the low- and high-RBM15 groups. **B** Correlation between immune cell infiltration and RBM15 expression. **C** Differences in immune cell infiltration between the low- and high-RBM15 groups. **D** Association of RBM15 with immune checkpoints. **E** IPS differences among patients with CTLA-4 or PD-1 expression in the low- and high-RBM15 groups. **F** Scatterplot depicting the correlation between RBM15 expression and the TMB

that RBM15 can influence PCa cell viability by regulating LINC02666 or AC022211.1 (Fig. S5).

Discussion

M6A, a prevalent chemical modification, can methylate RNA, thereby influencing its functionality [18, 19]. Previous studies have predominantly concentrated on the function of m6A in mRNA modification. However, m6A modification strongly influences the stability and functionality of lncRNAs. As post-transcriptional modifiers, lncRNAs regulate the progression of cancer through various mechanisms, thereby impacting tumor stage and prognosis [20, 21]. Studies have shown that the m6A modification of the lncRNA PCAT6

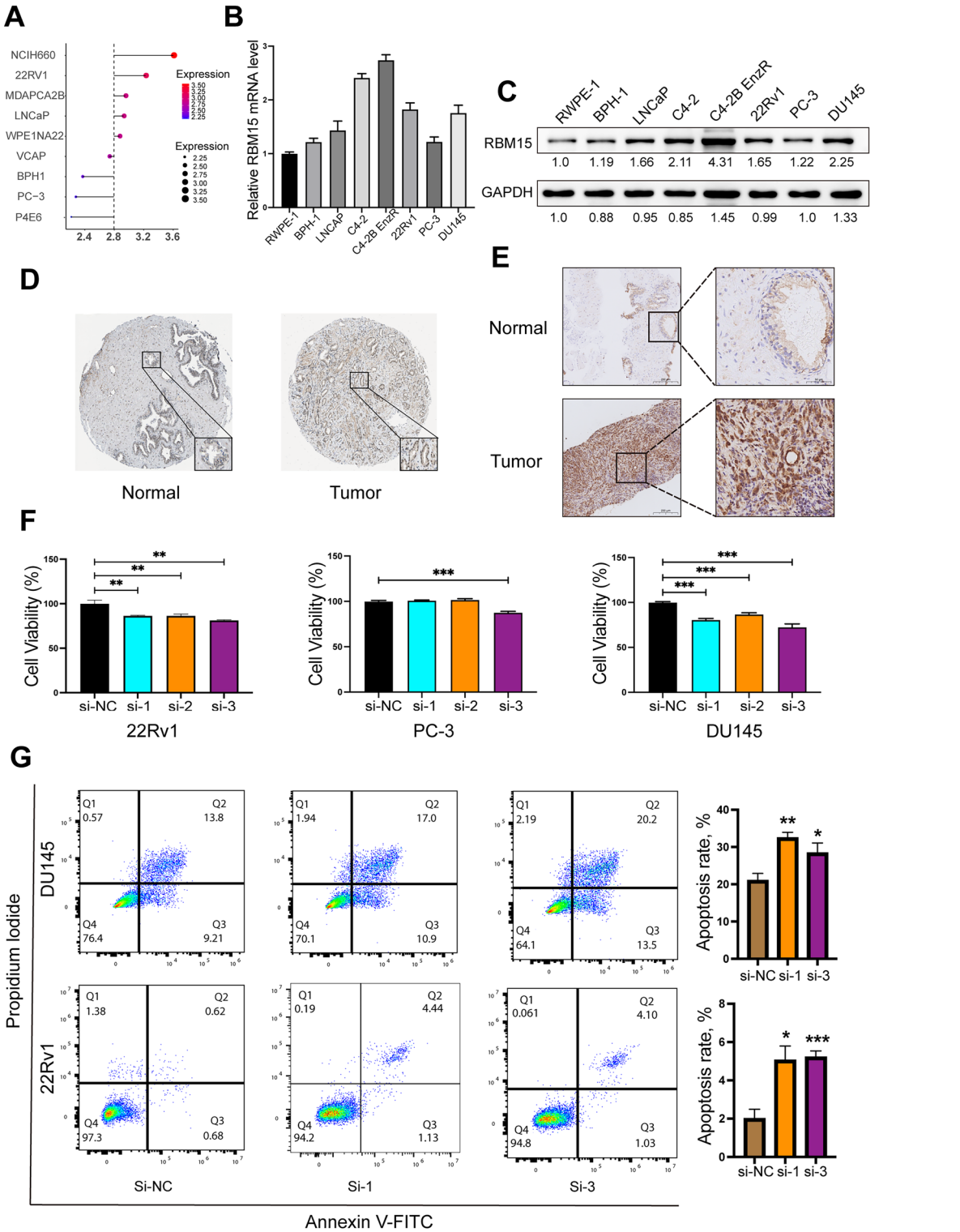

Fig. 7 Experimental validation of the role of RBM15 in PCa. **A** Analysis of RBM15 expression in PCa cells and normal prostate epithelial cells based on the CCLE database. **B** RT-qPCR illustrating the mRNA levels of RBM15 in PCa cells and normal prostate epithelial cells. **C** Western blot showing the protein levels of RBM15 in PCa cells and normal prostate epithelial cells. **D** IHC results from the HPA database demonstrating RBM15 expression in PCa and normal prostate tissue samples. **E** IHC results for surgical prostate tissue specimens indicating RBM15 expression in PCa and normal prostate tissue samples. **F** Changes in the viability of 22Rv1, PC-3, and DU145 cells following RBM15 knockdown. **G** Flow cytometry showing alterations in PCa cell apoptosis after RBM15 knockdown

promotes bone metastasis in PCa by stabilizing IGF1R mRNA via IGF2BP2, and a high PCAT6 level indicates an adverse patient outcome [22]. VIRMA-mediated m6A modification increases the stability and expression of the oncogenic lncRNAs CCAT1 and CCAT2, promotes PCa invasion and is correlated with poor prognosis [23]. Big data analysis, especially transcriptome or single-cell sequencing, facilitates the development of translational medicine [24]. In the present study, differentially expressed m6A-related lncRNAs between normal prostate and PCa tissues were identified based on the TCGA-PARD cohort. By employing LASSO regression analysis, a prognostic signature consisting of seven lncRNAs (AC105345.1, AL354989.1, AC138028.4, AC022211.1, AC020558.2, AC004076.2, and LINC02666) was constructed. The prognostic lncRNA-based risk score was associated with immune cell populations, as indicated by a positive association with naïve B cells, resting memory CD4+T cells, and activated mast cells but a negative association with resting mast cells. Overall, the prognostic risk signature was established to have a favorable predictive capacity for PCa outcomes and a strong correlation with immune cell abundance. Similarly, lncRNAs identified through comparable analytical methods have been indicated to be involved in immune regulation [6]. Notably, correlation analysis indicated a positive association between the m6A regulator RBM15 and the identified lncRNAs (AC004076.2, AL354989.1, LINC02666, and AC022211.1).

RBM15 and its paralog RBM15B lack catalytic functionality, but they can bind to the m6A methylation complex components METTL3 and WTAP, guiding them to carry out m6A modification at specific RNA sites [25, 26]. RBM15 recruits the m6A methyltransferase complex (referred to as the "writer") to mRNA by directly binding to RNA rich in uridine (U) sequences, mediating the occurrence of m6A modifications [26, 27]. m6A-binding proteins (referred to as "readers") recognize m6A modifications and affect RNA function in diverse processes, such as alternative splicing, stability, decay, and translation [28]. Mechanistically, RBM15 binds to m6A writers and readers through its conserved N-terminal SPOC domain, thus regulating m6A abundance and mRNA stability [29].

Currently, siRNA-mediated silencing of RBM15 significantly reduces the expression of the prognostic lncRNAs LINC02666 and AC022211.1 in PCa cells. The effectiveness of the siRNA knockdown strategy was confirmed using online tools (GeneScript siRNA Target Finder and BLAST) and western blot experiments. All three siRNA sequences targeting RBM15 were predicted to specifically target the RBM15 gene. The siRBM15-3 sequence was additionally predicted to target the FLT1 gene, but western blot experiments confirmed that FLT1 protein expression was not affected by this sequence (Fig. S6). High-RBM15 expression in PCa tissues was associated with an unfavorable prognosis. Subgroup analyses suggested that patients with increased age, aggravated Gleason score, and advanced pathological T and N stages exhibited dramatically amplified RBM15 expression. In addition, RBM15 has been implicated in the castration resistance of PCa. Moreover, individuals with elevated RBM15 expression may be sensitive to AMG-232 treatment. The MDM2 inhibitor AMG-232 impeded the MDM2-P53 interaction and activated P53 signaling to exert potent antitumor effects [30]. These effects could be reinforced through T-cell-mediated cytotoxicity against tumor cells [31]. Several clinical trials are also evaluating the therapeutic potential of AMG-232 in acute myeloid leukemia or various solid tumors [32, 33]. Hence, further experimental validation is needed to elucidate the interaction between AMG-232 and RBM15 to provide new insights into precision therapy strategies for PCa patients.

RBM15 is associated with tumor immunity and mutation burden [34]. Analysis of the TME indicated a high immune score in the high-RBM15 subgroup. Moreover, RBM15 expression was positively correlated with the abundance of resting memory CD4+T cells, activated mast cells, and naïve B cells but negatively correlated with the abundance of resting mast cells and activated NK cells. Notably, the immunophenoscore of patients with CTLA-4 and PD-1 double-negative expression differed significantly between the low- and high-RBM15 groups, suggesting that RBM15 may influence the immunotherapy responsiveness of patients in a specific subset. Furthermore, RBM15 expression was positively associated with TMB, suggesting that RBM15 may promote PCa incidence and progression. The expression pattern of RBM15 and its impact on the survival of PCa cells were further elucidated. Bioinformatic and experimental evidence showed that RBM15 expression in PCa cell lines was generally greater than that in non-tumor cells (RWPE-1 and BPH-1), with the highest expression observed in enzalutamide-resistant CRPC cells (C4-2B-EnzR), suggesting that RBM15 might be responsible for the castration resistance of PCa. IHC results of prostate specimens from public databases and experimental examination showed that PCa tissues had increased RBM15 expression in contrast to that in control normal tissues. Furthermore, RBM15 knockdown was sufficient to induce cell apoptosis and reduce cell viability in PCa cells, revealing the possible therapeutic benefits of RBM15 in PCa patients.

Only two studies have investigated the function of RBM15 in the context of prostate cancer to date.

LncRNA FTO-IT1 directly binds to RBM15 and acts as an inhibitor of the m6A writer complex METTL3-METTL14-WTAP-RBM15 to prevent m6A modification of p53-targeted genes, thus triggering the progression of PCa [35]. The complex formed between AZGP1P2 and UBA1/RBM15 mediates the ubiquitination and degradation of RBM15, hindering RBM15-mediated TPM1 mRNA methylation and decay, and thus enhancing the therapeutic effects of docetaxel on CRPC [36]. Nevertheless, these two investigations did not thoroughly explore the intricacies of RBM15 mechanisms. Additional clarification of the association between RBM15-associated m6A modification and PCa progression will enhance our understanding of the implications of RBM15 in cancer therapy.

Several studies have begun to explore the involvement of RBM15 in the m6A modification of lncRNAs. RBM15/15B recruits METTL3 to the m6A-modified lncRNA XIST and suppresses XIST-induced transcriptional silencing of genes on the X chromosome in a manner dependent on the m6A reader YTHDC1 [25]. Specifically, RBM15 selectively binds to the A-repeat region of the secondary structure of XIST, recruiting the writer complex for m6A modification, and the A-repeat (m6A) UCG tetraloop subsequently interacted with the Arc-like surface of the YTH domain [37]. RBM15, which functions by interacting with WTAP and METTL3, mediates the m6A modification of the lncRNA MALAT1, which serves as a molecular scaffold to interact with YTHDC1 to maintain the localization of nuclear speckles, inducing the expression of oncogenes and consequently promoting tumor cell migration [38]. Furthermore, lncRNAs can influence the function of RBM15. The lncRNA UBA6-AS1 can recruit RBM15 to facilitate m6A modification of UBA6 mRNA, after which the m6A reader IGF2BP1 binds to the m6A site and stabilizes UBA6 mRNA, thereby inhibiting the malignant activities of ovarian cancer cells [39]. Investigating the reciprocal interplay between lncRNAs and RBM15 could offer novel perspectives for PCa treatment and prognosis.

Overall, this study delineates the landscape of m6A-related lncRNAs in PCa. RBM15, an m6A writer, substantially influences the prognosis, clinical features, and tumor immunity of patients with PCa. RBM15 has emerged as an effective therapeutic target and a promising prognostic biomarker for PCa. However, this study has several limitations. First, the data used in this study were primarily sourced from the TCGA-PRAD cohort and GEO datasets, and additional external validation cohorts are essential for confirming the robustness of the results. Second, the current investigation revealed that RBM15 knockdown downregulates the expression of prognostic lncRNAs. Further in-depth elucidation of the direct m6A modification of these lncRNAs by RBM15 and the underlying mechanisms are needed. Finally, although preliminary results suggest that RBM15 can influence cell viability through m6A-related lncRNAs, it remains to be experimentally validated whether RBM15 affects PCa progression through alternative mechanisms.

Conclusion

This study delineated the landscape of m6A-related lncRNAs in PCa and determined a lncRNA-based risk signature for predicting PCa prognosis. Furthermore, the m6A methyltransferase RBM15 was identified and verified to be a critical regulator of prognostic lncRNAs and holds promise as a prognostic biomarker in PCa.

Abbreviations

LncRNA	Long noncoding RNA
M6A	N6-methyladenosine
PCa	Prostate cancer
TCGA	The Cancer Genome Atlas
CRPC	Castration-resistant prostate cancer
PSA	Prostate-specific antigen
LASSO	Least absolute shrinkage and selection operator
CDF	Cumulative distribution function
PCA	Principal component analysis
K-M	Kaplan–Meier
ROC	Receiver operating characteristic
TMB	Tumor mutation burden
IPS	Immunophenoscore
TCIA	The Cancer Immunome Atlas
HPA	Human Protein Atlas
CCLE	Cancer Cell Line Encyclopedia
KEGG	Kyoto Encyclopedia of Genes and Genomes
GO	Gene Ontology
FBS	Fetal bovine serum
siRNA	Small interfering RNA
ECL	Enhanced chemiluminescence
DEGs	Differentially expressed genes
TME	Tumor environment
FPKM	Fragments per kilobase of transcript per million mapped reads

Supplementary Information

The online version contains supplementary material available at https://doi.org/10.1186/s40001-024-02000-5.

Supplementary Material 1.

Supplementary Material 2. Figure S1: Determination of cluster numbers for m6A-related lncRNAs. Consensus clustering CDF with k ranging from 2 to 9. Relative changes in the area under the CDF curves for k = 2 to 9. Principal component analysis of the expression profiles within the two cluster patterns. Figure S2: Evaluation of the risk signature using prognostic m6A lncRNAs. Cross-validation of the LASSO model. PCA showing the distribution between the high- and low-risk groups. Figure S3: Expression of the DEGs and IC50 values of drugs in the subgroups with high- and low-RBM15 expression. Heatmap showing the DEGs between the high- and low-RBM15 groups. Boxplot demonstrating the differences in the IC50 values of the drugs Denileukin Diftitox Ontak, AMG-232, Nutlin-3, and MI-773 between the high- and low-RBM15 groups. Figure S4: Differential expression of RBM15 in different types of PCa. Differential expression of RBM15 between primary PCa and CRPC tissues. Differential expression of RBM15 between enzalutamide-sensitive and enzalutamide-resistant LNCaP or C4-2B cells. Figure S5: Effects of RBM15 knockdown or overexpression of LINC02666 or AC022211.1 on cell viability in 22Rv1 cells. Figure S6: The impact of siRNAs targeting RBM15 on the expression of FLT1 in

22Rv1 and DU145 cells. Figure S7: Transfection of Cy3-labeled siRNA in 22Rv1 and DU145 cells demonstrated high transfection efficiency.

Supplementary Material 3. Table S1: The sequences of siRNAs targeting RBM15 and the negative control. Table S2: Primer sequences for RT–qPCR. Table S3: The m6A regulators retrieved from the PubMed database. Table S4: Coefficients of 7 m6A-related lncRNAs in the LASSO regression analysis.

Acknowledgements
We sincerely thank the AJE team for their language polishing and editing of this manuscript, which made it clearer and more readable.

Author contributions
B.H. contributed to formal analysis, investigation, methodology, and original draft writing. D.L. and Z.L. performed the investigation, formal analysis, and result visualization. Y.W., R.C., and J.L. carried out project administration, supervision, and manuscript revising& editing. T.W. contributed to conceptualization, funding acquisition, and methodology. All authors have read and approved the final manuscript.

Funding
This work was supported by the Natural Science Foundation of Shenzhen City (grant number No. JCYJ20210324141404010).

Availability of data and materials
No datasets were generated or analysed during the current study.

Declarations

Ethics approval and consent to participate
The Ethics Committee of Tongji Hospital (TJ-IRB20221316) granted approval for this study.

Consent for publication
Not applicable.

Competing interests
The authors declare no competing interests.

Author details
[1]Department of Urology, Tongji Hospital, Tongji Medical College, Huazhong University of Science and Technology, Wuhan 430030, China. [2]Shenzhen Huazhong University of Science and Technology Research Institute, Shenzhen, Guangdong, China. [3]Department of Hepatic Surgery Center, Tongji Hospital, Tongji Medical College, Huazhong University of Science and Technology, Wuhan 430030, China.

Received: 18 March 2024 Accepted: 29 July 2024
Published online: 08 August 2024

References

1. Sung H, Ferlay J, Siegel RL, Laversanne M, Soerjomataram I, Jemal A, et al. Global cancer statistics 2020: GLOBOCAN estimates of incidence and mortality worldwide for 36 cancers in 185 countries. CA Cancer J Clin. 2021;71(3):209–49. https://doi.org/10.3322/caac.21660.
2. Schroder FH, Carter HB, Wolters T, van den Bergh RC, Gosselaar C, Bangma CH, et al. Early detection of prostate cancer in 2007. Part 1: PSA and PSA kinetics. Eur Urol. 2008;53(3):468–77. https://doi.org/10.1016/j.eururo.2007.10.047.
3. Flippot R, Beinse G, Boileve A, Vibert J, Malouf GG. Long non-coding RNAs in genitourinary malignancies: a whole new world. Nat Rev Urol. 2019;16(8):484–504. https://doi.org/10.1038/s41585-019-0195-1.
4. Liu SJ, Dang HX, Lim DA, Feng FY, Maher CA. Long noncoding RNAs in cancer metastasis. Nat Rev Cancer. 2021;21(7):446–60. https://doi.org/10.1038/s41568-021-00353-1.
5. Jiang W, Pan S, Chen X, Wang ZW, Zhu X. The role of lncRNAs and circRNAs in the PD-1/PD-L1 pathway in cancer immunotherapy. Mol Cancer. 2021;20(1):116. https://doi.org/10.1186/s12943-021-01406-7.
6. Zhang X, Ren L, Yan X, Shan Y, Liu L, Zhou J, et al. Identification of immune-related lncRNAs in periodontitis reveals regulation network of gene-lncRNA-pathway-immunocyte. Int Immunopharmacol. 2020;84:106600. https://doi.org/10.1016/j.intimp.2020.106600.
7. Li P, Ma X, Gu X. LncRNA MAFG-AS1 is involved in human cancer progression. Eur J Med Res. 2023;28(1):497. https://doi.org/10.1186/s40001-023-01486-9.
8. Amirmahani F, Ebrahimi N, Askandar RH, Rasouli Eshkaftaki M, Fazeli K, Hamblin MR. Long noncoding RNAs CAT2064 and CAT2042 may function as diagnostic biomarkers for prostate cancer by affecting target microrRNAs. Indian J Clin Biochem. 2021. https://doi.org/10.1007/s12291-021-00999-6.
9. Nasim E, Farzane A, Maryam A, Azin MG, Bahareh H. Two long non-coding RNAs, CAT179 and CAT1796, differentiate between benign prostate hyperplasia and prostate cancer. Arch Biol Sci. 2021;73(3):399–406. https://doi.org/10.2298/ABS210629033E.
10. Ma S, Chen C, Ji X, Liu J, Zhou Q, Wang G, et al. The interplay between m6A RNA methylation and noncoding RNA in cancer. J Hematol Oncol. 2019;12(1):121. https://doi.org/10.1186/s13045-019-0805-7.
11. Dominissini D, Moshitch-Moshkovitz S, Schwartz S, Salmon-Divon M, Ungar L, Osenberg S, et al. Topology of the human and mouse m6A RNA methylomes revealed by m6A-seq. Nature. 2012;485(7397):201–6. https://doi.org/10.1038/nature11112.
12. Shi H, Wei J, He C. Where, when, and how: context-dependent functions of RNA methylation writers, readers, and erasers. Mol Cell. 2019;74(4):640–50. https://doi.org/10.1016/j.molcel.2019.04.025.
13. Jiang X, Liu B, Nie Z, Duan L, Xiong Q, Jin Z, et al. The role of m6A modification in the biological functions and diseases. Signal Transduct Target Ther. 2021;6(1):74. https://doi.org/10.1038/s41392-020-00450-x.
14. Zhang X, Zhang S, Yan X, Shan Y, Liu L, Zhou J, et al. m6A regulator-mediated RNA methylation modification patterns are involved in immune microenvironment regulation of periodontitis. J Cell Mol Med. 2021;25(7):3634–45. https://doi.org/10.1111/jcmm.16469.
15. Newman AM, Liu CL, Green MR, Gentles AJ, Feng W, Xu Y, et al. Robust enumeration of cell subsets from tissue expression profiles. Nat Methods. 2015;12(5):453–7. https://doi.org/10.1038/nmeth.3337.
16. Yoshihara K, Shahmoradgoli M, Martinez E, Vegesna R, Kim H, Torres-Garcia W, et al. Inferring tumour purity and stromal and immune cell admixture from expression data. Nat Commun. 2013;4:2612. https://doi.org/10.1038/ncomms3612.
17. Reinhold WC, Sunshine M, Liu H, Varma S, Kohn KW, Morris J, et al. Cell Miner: a web-based suite of genomic and pharmacologic tools to explore transcript and drug patterns in the NCI-60 cell line set. Cancer Res. 2012;72(14):3499–511. https://doi.org/10.1158/0008-5472.CAN-12-1370.
18. Liu Z, Gao L, Cheng L, Lv G, Sun B, Wang G, et al. The roles of N6-methyladenosine and its target regulatory noncoding RNAs in tumors: classification, mechanisms, and potential therapeutic implications. Exp Mol Med. 2023;55(3):487–501. https://doi.org/10.1038/s12276-023-00944-y.
19. Jin Y, Fan Z. New insights into the interaction between m6A modification and lncRNA in cancer drug resistance. Cell Prolif. 2023. https://doi.org/10.1111/cpr.13578.
20. Amirmahani F, Vallian S, Asadi MH. The LncRNA MIAT is identified as a regulator of stemness-associated transcript in glioma. Mol Biol Rep. 2023;50(1):517–30. https://doi.org/10.1007/s11033-022-07962-5.
21. Oliayi AJ, Asadi MH, Amirmahani F. SNHG6 203 transcript could be applied as an auxiliary factor for more precise staging of breast cancer. J Kerman Univ Med Sci. 2019;26(4):253–9. https://doi.org/10.22062/jkmu.2019.89518.
22. Lang C, Yin C, Lin K, Li Y, Yang Q, Wu Z, et al. m(6) A modification of lncRNA PCAT6 promotes bone metastasis in prostate cancer through IGF2BP2-mediated IGF1R mRNA stabilization. Clin Transl Med. 2021;11(6):e426. https://doi.org/10.1002/ctm2.426.
23. Barros-Silva D, Lobo J, Guimaraes-Teixeira C, Carneiro I, Oliveira J, Martens-Uzunova ES, et al. VIRMA-dependent N6-methyladenosine modifications regulate the expression of long non-coding RNAs CCAT1 and CCAT2 in prostate cancer. Cancers (Basel). 2020. https://doi.org/10.3390/cancers12040771.

24. Amirmahani F, Ebrahimi N, Molaei F, Faghihkhorasani F, Jamshidi Goharrizi K, Mirtaghi SM, et al. Approaches for the integration of big data in translational medicine: single-cell and computational methods. Ann N Y Acad Sci. 2021;1493(1):3–28. https://doi.org/10.1111/nyas.14544.
25. Patil DP, Chen CK, Pickering BF, Chow A, Jackson C, Guttman M, et al. m(6)A RNA methylation promotes XIST-mediated transcriptional repression. Nature. 2016;537(7620):369–73. https://doi.org/10.1038/nature19342.
26. Knuckles P, Lence T, Haussmann IU, Jacob D, Kreim N, Carl SH, et al. Zc3h13/Flacc is required for adenosine methylation by bridging the mRNA-binding factor Rbm15/Spenito to the m(6)A machinery component Wtap/Fl(2)d. Genes Dev. 2018;32(5–6):415–29. https://doi.org/10.1101/gad.309146.117.
27. Jiang A, Zhang S, Wang X, Li D. RBM15 condensates modulate m(6)A modification of STYK1 to promote tumorigenesis. Comput Struct Biotechnol J. 2022;20:4825–36. https://doi.org/10.1016/j.csbj.2022.08.068.
28. Wang T, Kong S, Tao M, Ju S. The potential role of RNA N6-methyladenosine in Cancer progression. Mol Cancer. 2020;19(1):88. https://doi.org/10.1186/s12943-020-01204-7.
29. Appel LM, Franke V, Benedum J, Grishkovskaya I, Strobl X, Polyansky A, et al. The SPOC domain is a phosphoserine binding module that bridges transcription machinery with co- and post-transcriptional regulators. Nat Commun. 2023;14(1):166. https://doi.org/10.1038/s41467-023-35853-1.
30. Oh S, Lee MK, Chi SW. Single-molecule analysis of interaction between p53TAD and MDM2 using aerolysin nanopores. Chem Sci. 2021;12(16):5883–91. https://doi.org/10.1039/d1sc00386k.
31. Sahin I, Zhang S, Navaraj A, Zhou L, Dizon D, Safran H, et al. AMG-232 sensitizes high MDM2-expressing tumor cells to T-cell-mediated killing. Cell Death Discov. 2020;6:57. https://doi.org/10.1038/s41420-020-0292-1.
32. Erba HP, Becker PS, Shami PJ, Grunwald MR, Flesher DL, Zhu M, et al. Phase 1b study of the MDM2 inhibitor AMG 232 with or without trametinib in relapsed/refractory acute myeloid leukemia. Blood Adv. 2019;3(13):1939–49. https://doi.org/10.1182/bloodadvances.2019030916.
33. Rozeboom B, Dey N, De P. ER+ metastatic breast cancer: past, present, and a prescription for an apoptosis-targeted future. Am J Cancer Res. 2019;9(12):2821–31.
34. Zhao Z, Ju Q, Ji J, Li Y, Zhao Y. N6-methyladenosine methylation regulator RBM15 is a potential prognostic biomarker and promotes cell proliferation in pancreatic adenocarcinoma. Front Mol Biosci. 2022;9: 842833. https://doi.org/10.3389/fmolb.2022.842833.
35. Zhang J, Wei J, Sun R, Sheng H, Yin K, Pan Y, et al. A lncRNA from the FTO locus acts as a suppressor of the m(6)A writer complex and p53 tumor suppression signaling. Mol Cell. 2023;83(15):2692-708.e7. https://doi.org/10.1016/j.molcel.2023.06.024.
36. Wang H, Liu J, Zhu X, Yang B, He Z, Yao X. AZGP1P2/UBA1/RBM15 cascade mediates the fate determinations of prostate cancer stem cells and promotes therapeutic effect of docetaxel in castration-resistant prostate cancer via TPM1 m6A modification. Research (Wash D C). 2023;6:0252. https://doi.org/10.34133/research.0252.
37. Jones AN, Tikhaia E, Mourão A, Sattler M. Structural effects of m6A modification of the Xist A-repeat AUCG tetraloop andits recognition by YTHDC1. Nucleic Acids Res. 2022;50(4):2350–62. https://doi.org/10.1093/nar/gkac080.
38. Wang X, Liu C, Zhang S, Yan H, Zhang L, Jiang A, et al. N(6)-methyladenosine modification of MALAT1 promotes metastasis via reshaping nuclear speckles. Dev Cell. 2021;56(5):702-15.e8. https://doi.org/10.1016/j.devcel.2021.01.015.
39. Wang Y, Chen Z. Long noncoding RNA UBA6-AS1 inhibits the malignancy of ovarian cancer cells via suppressing the decay of UBA6 mRNA. Bioengineered. 2022;13(1):178–89. https://doi.org/10.1080/21655979.2021.2011640.

Publisher's Note